Specnuezhenide from Ligustrum sinense Lour. inhibits liver cancer by suppressing glycolysis: a multi-omics study

Zongchao Hong

zchong369@163.com

Hubei Minzu University, China

Jingxin Yang

Hubei Minzu University, China

Wanjin Sun

Hubei Provincial Hospital of Traditional Chinese Medicine

Chenhuan Jin

Hubei Minzu University, China

Baodan Hu

The Central Hospital of Enshi Tujia and Miao Autonomous Prefecture

Houcong Li

Hubei Minzu University, China

Jiajun Wang

Hubei Minzu University, China

Xueyun Duan

Hubei Provincial Hospital of Traditional Chinese Medicine

Article

Keywords: Ligustrum sinense Lour., Liver cancer, Glycolysis, Specnuezhenide

Posted Date: March 5th, 2026

DOI: https://doi.org/10.21203/rs.3.rs-8455901/v1

Additional Declarations: No competing interests reported.

Specnuezhenide from *Ligustrum sinense* Lour. inhibits liver cancer by suppressing glycolysis: a multi-omics study

Zongchao Hong[a,b,c#*], Jingxin Yang[b#], Wanjin Sun[e#], Chenghuan Jin[b], Baodan Hu[d], Houcong Li[b], Jiajun Wang[b*], Xueyun Duan[e*]

[a] *Wuling Mountain Traditional Chinese Medicine Inspection and Testing Center, Hubei Minzu University, Enshi, China.*

[b] *Health Science Center，Hubei Minzu University, Enshi, China.*

[c] *Hubei Provincial Key Laboratory of Occurrence and Intervention of Rheumatic diseases，Hubei Minzu University, Enshi, China.*

[d] *The Central Hospital of Enshi Tujia and Miao Autonomous Prefecture, Enshi, China.*

[e] *Hubei Key Laboratory of theory and application research of liver and kidney in traditional Chinese medicine, Hubei Provincial Hospital of Traditional Chinese Medicine, Wuhan, China.*

[#]These authors contributed equally to this work.

[*]**Corresponding author**

Zongchao Hong: ZCHong369@163.com

Jiajun Wang: wangjiajunzhch@126.com

Xueyun Duan: xueyunduan@sina.com

Hubei Minzu University, 39 Xueyuan Road, Enshi 445000, Hubei, China.

Abstract:

This study investigates the anti-liver cancer mechanism of *Ligustrum sinens*e Lour. (XDQ), a Tujia ethnomedicine, using a multi-omics approach. In H22 tumor-bearing mice, XDQ significantly inhibited tumor growth by up to 79.64% without observable toxicity. UPLC-Q/TOF-MS analysis identified 66 compounds in XDQ, with five—specnuezhenide, prosapogenin A, oleuropein, oxyberberine, and pseudoanisatin—detected in both serum and tumor tissues, indicating good bioavailability. Integrated network pharmacology, transcriptomics, and proteomics analyses consistently revealed that XDQ's anti-tumor effect is mediated through the suppression of glycolysis. This was evidenced by the downregulation of key glycolytic enzymes, including GPI, PGAM1, PGK1, and PKM2, and a subsequent decrease in glucose consumption and lactate production. Molecular docking identified specnuezhenide as the component with the strongest binding affinity to the rate-limiting enzyme GPI. In vitro validation confirmed that specnuezhenide inhibits glycolysis and suppresses the expression of glycolysis enzymes in liver cancer cells. Our findings demonstrate that XDQ exerts its anti-liver cancer effects primarily by inhibiting tumor glycolysis, with specnuezhenide being a key active constituent, providing a scientific basis for developing XDQ as a potential therapeutic agent.

Keywords: *Ligustrum sinense* Lour.; Liver cancer; Glycolysis; Specnuezhenide

Abbreviations

ALT: Alanine aminotransferase; AST: Aspartate Aminotransferase; BP: Biological process; BUN: Blood Urea Nitrogen; Cr: Creatinine; DEGs: Differentially expressed genes; ENO1: Enolase 1; ENO3: Enolase 3; FA: Formic acid; GLUT: Glucose transporter; GO: Gene Ontology; GPI: Glucose-6-phosphate isomerase; HK: Hexokinase; KEGG: Kyoto Encyclopedia of Genes and Genomes; LDHA: L-lactate dehydrogenase A chain; MF: Molecular function; PFK: ATP-dependent 6-phosphofructokinase; PGAM1: Phosphoglycerate mutase 1; PGK1: Phosphoglycerate kinase 1; PKM2: Pyruvate kinase; UA: Urine acid.

1. Introduction

Hepatocellular carcinoma, the predominant form of primary liver cancer, poses a severe and escalating health challenge globally [1]. Recent GLOBOCAN estimates suggest liver cancer to be the third leading cause of cancer-related mortality worldwide, with over 900,000 new cases and 830,000 deaths annually, disproportionately affecting regions of Eastern Asia and Africa [2]. Despite advances such as surgical resection, targeted agents (e.g., sorafenib, lenvatinib), and immunotherapies, the prognosis for advanced liver cancer remains dismal, with 5-year survival rates being less than 20% [3]. This therapeutic failure is largely attributable to intrinsic and acquired drug resistance, high rates of metastatic recurrence, and significant treatment-related toxicities. The disease burden of liver cancer is particularly acute in China, with an incidence of approximately 45% of global cases [4]. The age-standardized incidence rates in high-risk Chinese regions reach 28.3 per 100,000, which is nearly triple the global average, with a pronounced male predominance (male-to-female ratio >2.5:1). Chronic hepatitis B virus (HBV) infections remain the primary etiological driver and are implicated in more than 60% of cases, synergistically exacerbated by exposure to dietary aflatoxin, the increasing prevalence of metabolic dysfunction–associated steatotic liver disease (MASLD), and alcohol abuse. Despite substantial public health efforts, including nationwide HBV

vaccination and antiviral therapy programs, liver cancer persists as the second leading cause of cancer-related deaths in China, with a 5-year relative survival rate of merely 12.1% for advanced-stage disease [5]. These stark limitations underscore the urgent need to identify safer and more efficacious therapeutic strategies to treat liver cancer.

Traditional herbal medicines, characterized by their multicomponent and multitarget nature, show promise in cancer chemoprevention and as adjuvant therapy. Ethnomedicines, particularly those derived from indigenous systems such as Tujia medicine in China, are rich repositories of biologically active compounds, with their therapeutic potential having been empirically validated through centuries of use [6]. These understudied ethnopharmacological resources could be a valuable source for discovering novel chemical scaffolds in an era of high attrition rates in conventional drug discovery. *Ligustrum sinense* Lour., known as "Xiaodongqing" (XDQ) in Tujia ethnomedicine, has a documented history of use in treating inflammation, fever, and viral infections with a favorable safety profile [7]. Modern phytochemical analyses have confirmed that XDQ contains diverse bioactive constituents such as terpenoids (e.g., oleanolic acid), lignans (e.g., phillygenin), flavonoids (e.g., luteolin), iridoids, and phenylethanoid glycosides. The extracts and isolated compounds of XDQ, or botanically related species, have demonstrated a range of pharmacological activities, including anti-inflammatory, analgesic, antioxidant, hepatoprotective, antibacterial, and anticancer effects in preliminary studies [8]. However, despite its traditional use and the known bioactivity of its chemical constituents, systematic investigations into the specific pharmacodynamic substances responsible for the overall effect of XDQ and the integrated molecular mechanisms underlying its systemic anti–liver cancer effect remain largely unexplored, significantly hindering its clinical translation.

Elucidation of the complex molecular mechanisms of botanical drugs necessitates precise identification of their chemical constituents and determining their biological interactions. To address the dual challenges of the unresolved active components and undefined anti-liver cancer mechanisms of XDQ, and driven by the critical need to identify novel therapeutics to treat liver cancer, an integrated multiomics strategy was adopted in this study to elucidate the XDQ-regulated

therapeutic network in the treatment of liver cancer. Our preliminary analyses suggest that the anti‑liver cancer effect of XDQ may be closely related to the regulation of glycolysis, which are critically implicated in the pathogenesis, progression, and drug resistance in liver cancer. Our findings not only scientifically validate the clinical potential of Tujia ethnomedicine but also significantly expand the chemical and mechanistic resources available for the discovery of anti-liver cancer drugs. The key active ingredients of XDQ were identified in this study, establishing a crucial foundation for its standardization, quality control, and comprehensive utilization.

2. Materials and Methods

2.1 Reagents and materials

XDQ, sourced from Enshi, Hubei Province, China, was verified by Dr. Houcong Li. Approximately 100 g of the material was sliced, soaked in 800 mL of water for 2 h, boiled, and simmered for 1.5 h. The extract was filtered, and the residue was re-extracted with 500 mL of water. The filtrates were combined and concentrated to 250 mL, and a 0.4 g/mL stock solution was prepared. Acetonitrile (Cat. No. 1.00030.4008), methanol (Cat. No. 1.06007.4008), and formic acid (Cat. No. 111670) were purchased from Millipore (Bedford, MA, USA). Ethanol (Cat. No. 10009218) was purchased from Sinopharm Chemical Reagent Co., Ltd. (Shanghai, China). Details of the reagent kits, antibodies, and other consumables used in this study are summarized in Table S1 in the Supplementary Material.

2.2 *In vivo* experiments

The H22 hepatoma cell line (Cat No. CL-0341; Procell Life Science & Technology Co., Ltd., Wuhan, China) was used to establish tumor-bearing mouse models in male Balb/c mice (8 weeks old, SPF grade, 17–20 g body weight, supplied by the Experimental Animal Center of China Three Gorges University). Successfully modeled mice were divided into a model group, two positive control groups (Adriamycin and Huaier granules), and high-, medium-, and low-dose XDQ treatment groups, in addition to a normal control group (n=10 per group). Based on the prescription and clinical medication experience, the following doses were used for

intervention: Huaier granules, 7.8 g/kg/d; Adriamycin, 2 mg/kg/3d; XDQ high-dose group, 4.0 g/kg/d; XDQ medium-dose group, 2.0 g/kg/d; XDQ low-dose group, 1.0 g/kg/d. Adriamycin was administered through intraperitoneal injections, while the remaining drugs were administered by gavage according to the body weight of mice. Mice in the normal group were administered the same volume of physiological saline by gavage. After 10 days of continuous administration, anesthesia was administered by intraperitoneal injection of avertin at a dose of 1000 mg/kg body weight. Serum, tumor tissues, and organs of mice were collected to determine the tumor weight and levels of the related indicators. All animal procedures were conducted in accordance with relevant ethical guidelines and were approved by the Animal Research Committee of Hubei Minzu University (Approval No. 202271, December 31, 2022). The study complied with the ARRIVE guidelines for reporting in vivo experiments. Ethical approval was obtained as part of a broader project under which multiple related studies are reported.

The tumor inhibition rate for each treatment group was calculated as follows: Tumor Inhibition Rate (%) = [(A − B) / A] × 100%, where A is the average tumor weight in the model group and B is the average tumor weight in the experimental group.

2.3 Component analysis

The components of XDQ were analyzed using UPLC-Q/TOF-MS linked to an ACQUITY UPLC® HSS T3 column (2.1 × 100 mm, 1.8 μm) (Waters, Milford, MA, USA). The following parameters were used: injection volume, 10 μL; column temperature, 40°C; flow rate, 0.3 mL/min. The chromatographic separation utilized a mobile phase of 0.1% formic acid in water (A) and 0.1% formic acid in acetonitrile (B) with the following gradient program: 0 – 2 min, 0% B; 2 – 4 min, 25% B; 4 – 22 min, 25 – 100% B (linear); 22 – 25 min, 100% B; 25 – 25.1 min, 100 – 0% B (linear); 25.1 – 30 min, 0% B for column re-equilibration.

Following UPLC separation, samples were analyzed by UPLC-ESI-MS/MS using a Q Exactive Plus mass spectrometer (Thermo Scientific) equipped with a heated electrospray ionization (H-ESI) source. Each sample was analyzed separately

in both positive and negative ESI modes. Ionization parameters were configured with positive and negative spray voltages set to 3.8 kV (+) and 3.2 kV (-) , respectively. The capillary was maintained at 320℃, while the probe heater temperature was set to 350℃. Sheath gas flow was adjusted to 30 arbitrary units, with an auxiliary gas flow of 5 units. The S-Lens RF level was maintained at 50.

2.4 Network pharmacology

XDQ extracts, rat serum, and liver cancer tissues were analyzed using UPLC-Q/TOF-MS, and the components entering the blood and target organs were identified and used for network pharmacology analysis. The identified components were obtained in the .sdf format from PubChem (https://pubchem.ncbi.nlm.nih.gov) and uploaded to PharmMapper (https://lilab-ecust.cn/pharmmapper/) to obtain predicted targets. The term "liver cancer" was used as a keyword to obtain disease-related genes from GeneCards (http://www.genecards.org). Venn analysis was used to identify the overlapping targets between liver cancer‐related genes and drug-active components. These intersection targets were submitted to the STRING database (https://string-db.org/) to construct a protein‐protein interaction network, which was visualized using Cytoscape 3.10.1 (https://cytoscape.org/). Gene Ontology (GO) annotation and Kyoto Encyclopedia of Genes and Genomes (KEGG) pathway enrichment analyses for the overlapping targets were performed based on the STRING database.

2.5 Determination of biochemical indices

Alanine aminotransferase (ALT), aspartate aminotransferase (AST), blood urea nitrogen (BUN), creatinine, uric acid, and glucose, lactate were used following the manufacturers' instructions to determine the content of these metabolites.

2.6 Transcriptome sequencing

Total ribonucleic acid (RNA) was extracted from liver cancer tissues using the TRIzol method, and eukaryotic mRNA was enriched using magnetic beads with Oligo (dT). Next, a fragmentation buffer was added to randomly interrupt the messenger RNA (mRNA). Using mRNA as a template, the first complementary deoxyribonucleic acid (cDNA) strand was synthesized using random hexamer primers.

Then, buffer, deoxynucleotide triphosphates, and DNA polymerase I were added to synthesize the second cDNA strand. The double-stranded cDNA was purified using AMPure XP beads and enriched using polymerase chain reaction to obtain the final cDNA library. Different libraries were pooled according to the target sequencing data volume and sequenced on the machine. Transcriptome sequencing was performed in collaboration with Applied Protein Technology. The differentially expressed genes were screened using fold change (FC) = 2 as the threshold.

2.7 Proteomics analysis

Proteomics analysis was conducted in collaboration with Shanghai Bioprofile. The method that was used is briefly described.

Protein extraction and digestion

Protein samples were prepared using the following procedure. Tissue specimens were mechanically disrupted in 200 μL of a lysis solution containing 4% SDS, 100 mM DTT, and 150 mM Tris-HCl (pH 8.0). The homogenate was first heated at 100°C for 5 minutes, subjected to sonication, and then heated again under the same conditions. Following centrifugation at 16,000 ×g for 15 minutes, the supernatant was recovered. Protein content was quantified via a BCA assay.

To purify the protein extract, detergent and other small molecules were eliminated through sequential ultrafiltration (30 kDa molecular weight cutoff) with UA buffer (8 M urea, 150 mM Tris-HCl, pH 8.0). Subsequently, cysteine reduction was performed with DTT, followed by alkylation using 50 mM iodoacetamide in UA buffer for 20 minutes in darkness. The filters were then rinsed with UA buffer and 25 mM ammonium bicarbonate. Protein digestion was carried out with trypsin (enzyme-to-substrate ratio of 1:25) in 25 mM NH_4HCO_3 at 37°C for approximately 16 hours. Finally, the resulting peptides in the filtrate were collected, and their concentration was assessed by measuring the absorbance at 280 nm.

Tandem mass tag (TMT) labeling

For peptide labeling, 100 μg aliquots were processed with TMT reagents (Thermo Fisher Scientific) following the supplier's instructions. In brief, peptides were dissolved in 50 mM triethylammonium bicarbonate (pH 8.5) and combined with

the TMT label dissolved in anhydrous acetonitrile, followed by incubation for 1 hour at ambient temperature. The labeling reaction was terminated by adding 5% hydroxylamine for 15 minutes. All labeled samples were then combined into one pool and dried under vacuum.

Fractionation at high pH

The pooled TMT-labeled peptides were separated by high-pH reversed-phase chromatography using an Agilent 1290 HPLC system equipped with a Waters XBridge BEH130 C_{18} column (2.1 × 150 mm, 3.5 μm). Separation was performed with a gradient established between mobile phase A (10 mM ammonium formate, pH 10) and mobile phase B (10 mM ammonium formate in 90% acetonitrile, pH 10), at a constant flow rate of 0.3 mL/min. A total of 30 fractions were collected, which were subsequently consolidated into 15 fractions, concentrated, and dried for downstream LC-MS/MS analysis.

LC-MS/MS

Peptides were separated in a C_{18} column packed in-house (75 μm internal diameter, particle size 3 μm) using an Easy nLC system coupled to a Q-Exactive mass spectrometer (Thermo Fisher Scientific). A 90-min linear gradient of buffer A (0.1% formic acid, 2% acetonitrile) to buffer B (0.1% formic acid, 90% acetonitrile) at 300 nL/min was used for separation. Mass spectrometry (MS) data were acquired in data-dependent mode: full MS scans (70000 resolution, *m/z* 300–1800) were followed by higher-energy collisional dissociation fragmentation (normalized collision energy [NCE] 30%) of the top 15 most intense precursors (MS/MS resolution 35000). Automatic gain control targets were $1e^6$ (MS, max IT 50 ms) and $1e^5$ (MS/MS, max IT 100 ms). Dynamic exclusion was set to 30 s.

Data analysis

Raw data were processed using Proteome Discoverer 2.4 (Thermo Fisher Scientific), and differentially expressed proteins (DEPs) were identified using Perseus software with thresholds of FC > 1.20 or < 0.83 and p-value < 0.05. DEPs were analyzed by hierarchical clustering and used for GO and KEGG enrichment analyses.

2.8 Molecular Docking

The three-dimensional structures of the compounds in ".sdf" format were obtained from the PubChem database (https://pubchem.ncbi.nlm.nih.gov/). Corresponding protein structures were retrieved from the RCSB Protein Data Bank (https://www.rcsb.org/). Using Discovery Studio 2019 software (BIOVIA, San Diego, USA), all protein structures were prepared by removing solvent molecules and original ligands, followed by hydrogenation and the addition of partial charges. Molecular docking was performed using AutoDock software to evaluate the binding potential of the compounds to the target proteins. A LibDockScore greater than 100 was considered indicative of a likely interaction, with higher scores reflecting stronger predicted binding affinity.

2.9 Cell culture

HuH7 and Li-7 cell lines were obtained from Procell Life Science & Technology Co., Ltd. (Wuhan, China). Cells were maintained in RPMI-1640 medium supplemented with 10% fetal bovine serum and 1% penicillin–streptomycin at 37 °C in a humidified incubator with 5% CO_2. Cell viability was assessed using an MTT assay according to the manufacturer's protocol.

2.10 Western blotting

Total protein was isolated from tissue and cell specimens using an appropriate lysis buffer, and concentrations were determined with a BCA assay kit. After quantification, protein samples were denatured by heating to 100°C. For each sample, a 20 μg aliquot was loaded and separated by SDS-PAGE, followed by electrophoretic transfer onto a PVDF membrane.

The membranes were blocked for 1.5 hours at room temperature with 5% non-fat dry milk prepared in Tris-buffered saline. Subsequently, they were incubated with specific primary antibodies overnight at 4°C. Following three washes with TBST, the membranes were incubated for one hour at room temperature with horseradish peroxidase (HRP)-conjugated secondary antibodies [24]. After three more washes with TBST, the protein bands were visualized using enhanced chemiluminescence reagent and imaged.

2.11 Statistical analysis

GraphPad Prism 10.1 and Origin 2021 were used for data analyses. Differences were considered statistically significant at $p < 0.05$. Data are presented as mean±standard deviation. Differences between two groups were determined using independent sample *t*-tests, whereas differences between two or more groups were determined using one-way analysis of variance.

3. Results

3.1 XDQ has anti-tumor activity *in vivo*

XDQ is a nontoxic natural medicine. A tumor-bearing mouse model was established in this study to evaluate the *in vivo* anti-tumor effects of XDQ (Figure 1A). Adriamycin, a chemotherapeutic agent to treat liver cancer, and Huaier granules, a Chinese patent medicine commonly used to treat liver cancer, were used as the positive controls. Mice in the high-dose XDQ group demonstrated a tumor growth–inhibition rate of 79.64%, which was marginally lower by 4% compared with that of Adriamycin (83.67%). Conversely, mice in the medium-dose XDQ group exhibited a tumor growth–inhibition rate of 67.52%, which was significantly higher than that observed using Huaier granules (43.57%). Mice in the low-dose XDQ group demonstrated a tumor growth–inhibition rate of 40.68% (Figure 1B). These findings are suggestive of the *in vivo* anti-tumor effect of XDQ. No significant differences in serum ALT and AST levels were noted between the XDQ-treated group and the normal control group. However, significant improvements were observed in urea nitrogen, creatinine, and uric acid levels after XDQ intervention (Figure 1C, D, E, F, G). Furthermore, analysis of the organ coefficients of the liver, spleen, kidneys, and heart of mice indicated that adriamycin may induce organ atrophy, whereas XDQ did not cause organ damage (Figure 1H, I, J, K). These results suggest that XDQ has anti-liver cancer efficacy *in vivo* without any adverse side effects.

3.2 Screening and characterization of the active fractions in XDQ

XDQ decoction was administered to model mice with liver cancer via gavage. Subsequently, the serum and tumor tissue samples were collected and analyzed using

UPLC-Q/TOF-MS (Figures 2, 3, 4). A total of 66 chemical constituents including oleuropein, aesculatin, specnuezhenide, prosapogenin A (Table 1 in the supplementary material) and several compounds with diverse physiological activities such as phenols, flavonoids, Prenol lipids, and alkaloids (Figure 2B) were identified based on comprehensive analysis and testing of the XDQ decoction. After XDQ intervention, 9 components were detected in the blood of mice, with 7 components including prenol lipids, alkaloids, flavonoids, furanoid lignans, and others (Figure 2C) penetrating liver cancer tissues. The therapeutic efficacy of a drug is contingent upon its ability to reach the target organ through the bloodstream and traverse biological membranes. Consequently, the compounds that are present in both the bloodstream and the target organs are the likely candidates that can exert their therapeutic effects [9]. Of particular interest, 5 components in XDQ were identified in both the blood and liver cancer tissues, suggesting them to be the active ingredients responsible for the anti–liver cancer effect of XDQ (Figure 5A, Table 2).

3.3 Network pharmacology

179 potential targets for 5 compounds were predicted using the PharmMapper database (Table S2 in the Supplementary Material), and an XDQ-component -targets network was plotted (Figure 5B) . More than 50000 liver cancer–associated targets were retrieved from the GeneCards database, and the top 1000 targets were subsequently selected for further analysiss, and 57 of them were identified as potential targets of five compounds (Figure 5C, Table S3 in the Supplementary Material). The interactions among these targets are complex (Figure 5D) and frequently involve biological processes (BP) such as response to organic cyclic compound, response to endogenous stimulus, regulation of programmed cell death, regulation of molecular function, and regulation of metabolic process. Additionally, they encompass molecular functions (MF) including small molecule binding, protein kinase activity, protein binding, and nuclear receptor activity (Figure 5E). The enriched KEGG pathways that were identified included pathways in cancer, PI3K-Akt signaling pathway, hepatocellular carcinoma, apoptosis, and glycolysis/gluconeogenesis (Figure 5F). It is worth noting that among the five screened components, specnuezhenide,

prosapogenin A, and oleuropein are all related to glycolysis (Figure 5G). These findings suggested that the inhibitory effect of XDQ on liver cancer may be mediated via the regulation of glycolysis, and the key components that play a major role may be specnuezhenide, prosapogen A, and oleuropein.

3.4 Transcriptome analysis of the anti–liver cancer mechanism of XDQ

Upon confirming the active constituents of XDQ and its efficacy against liver cancer, its underlying mechanism of action was elucidated. Transcriptome sequencing analysis demonstrated that XDQ intervention significantly altered the expression of 1584 genes in tumor tissues, with 1424 genes being upregulated and 160 genes being downregulated (Figure 6A, B). GO enrichment analysis of these DEGs led to the identification of BP categories, such as immune response and defense response, as well as MF categories including protein binding, molecular transducer activity, and immune receptor activity (Figure 6C). Directed acyclic graph analysis of the BP terms indicated immune response and defense response as the ultimate functional outcomes (Figure 6D), suggesting immunomodulation as the likely pivotal pathway for the anti-tumor effects of XDQ. KEGG pathway enrichment analysis led to the identification of several pathways related to energy metabolism, including taurine and hypotaurine metabolism, arachidonic acid metabolism, and glycolysis/gluconeogenesis (Figure 6E). Notably, identification of the glycolysis/gluconeogenesis pathway in the transcriptomic analysis corroborated the predictions from network pharmacology. Furthermore, the majority of enzymes involved in the glycolysis/gluconeogenesis pathway, including key rate-limiting enzymes such as phosphoglucomutase 2 (PGM2) and glucose-6-phosphate isomerase (GPI), were inhibited following XDQ intervention (Figure 6F).

3.5 Proteomic analysis of the anti–liver cancer mechanism of XDQ

Proteomics analysis led to the identification of more than 6500 proteins in tumor tissues (Figure 7A). XDQ leads to 503 differentially expressed proteins (DEPs) in tumor tissue, with 301 proteins being upregulated and 202 being downregulated after XDQ intervention (Figure 7B, C). Importantly, 172 of these DEPs were associated with glycolysis (Figure 7D). GO enrichment analysis indicated these DEPs to be

primarily involved in biological regulation and metabolic regulation and predominantly associated with MFs such as protein binding, organic cyclic compound binding, and ion binding (Figure 7E). Findings from KEGG pathway enrichment analysis demonstrated the participation of the 503 DEPs in regulating pathways including amino acid metabolism, carbohydrate metabolism, and glycan biosynthesis and metabolism. Excitingly, glycolysis/glycogenesis was once again enriched (Figure 7F). This forces us to focus on the molecular mechanism of XDQ's anti-liver cancer effect on glycolysis.

3.6 XDQ inhibits glycolysis in liver cancer

To further elucidate the impact of XDQ on tumor glycolysis, we measured the expression of several key catalytic enzymes in the glycolysis pathway. As expected, the intervention of XDQ could downregulate the expression of GPI, PGAM1, PGK1, and PKM2 in tumor tissues (Figure 8A). It is obvious that after XDQ treatment, the glucose consumption and lactic acid production of the tumor also decreased significantly (Figure 8B), which further indicates the decline in glycolysis activity in the tumor. In addition, we reanalyzed the key glycolysis markers identified in the transcriptomic and proteomic datasets. The expression of several glycolysis enzymes, including Eno3, Pgam2, Pfkm, Aldoa, Eno2, Ldha, and Pgk1, was found to be suppressed at the protein level (Figure 8C), which is consistent with the results we detected. Furthermore, hexokinase (HK), which catalyzes the conversion of glucose to glucose-6-phosphate, was significantly upregulated following XDQ intervention, whereas the downstream rate-limiting glycolysis enzyme GPI was markedly suppressed. This suggests that the primary target of XDQ is unlikely to be HK or any upstream factors, but rather that it attenuates glycolysis flux through inhibition of GPI.

3.7 Specnuezhenide derived from XDQ can inhibit glycolysis in liver cancer

Previous research has identified specnuezhenide, prosapogenin A, oleuropein, oxyberberine, and pseudoanisatin as components of XDQ that directly penetrate the bloodstream and tumor tissues, suggesting their potential role as active agents in the inhibition of glycolysis by XDQ. The suppression of glycolysis by XDQ is likely

mediated through the inhibition of the rate-limiting enzyme GPI. To elucidate which specific substances in XDQ target GPI, molecular docking techniques were employed to predict the binding affinities between the five compounds and GPI. The LibDock scores for specnuezhenide, prosapogenin A, and oleuropein with GPI all exceeded 100 (Table 3), with the primary binding interactions being conventional hydrogen bonds, carbon-hydrogen bonds, and Pi-Pi T-shaped interactions (Figure 9A, B, C). Notably, the LibDock score for specnuezhenide with GPI was 176.613, indicating its superior binding potential and suggesting that it may be a critical component of XDQ in targeting GPI to inhibit glycolysis.

At the cellular level, specifically in Huh7 and Li-7 cells, a concentration of 50 μM specnuezhenide exhibited a notable inhibitory effect (Figure 10A, B). Subsequent analysis of the culture medium revealed that treatment with 100 μM specnuezhenide resulted in an increased glucose concentration and a decreased lactic acid concentration (Figure 10C, D). This suggests that specnuezhenide impedes glucose uptake and lactic acid production in tumor cells. Moreover, specnuezhenide intervention was found to suppress the expression of glycolytic enzymes GPI, PGAM1, PGK1, and PKM2 in both Huh7 and Li-7 cells (Figure 10E, F). Collectively, these findings suggest that specnuezhenide effectively inhibits tumor glycolysis and plays a critical role for XDQ targeting GPI to hinder glycolysis, thereby contributing to the suppression of tumor progression.

In summary, our integrated multi-omics analyses and subsequent validation confirm that the anti-tumor effect of XDQ is mediated through the suppression of glycolysis. Notably, XDQ, particularly its active constituent specnuezhenide, effectively intervenes by impeding glucose uptake, suppressing the glycolysis rate-limiting enzyme GPI, diminishing lactate production, and ultimately inhibiting glycolysis, thereby attenuating tumor proliferation (Figure 8D).

4. Discussion

A hallmark of cancer metabolic reprogramming is the distinct preference of tumor cells for converting glucose to lactate via glycolysis, even in the presence of

adequate oxygen, rather than utilizing the more energetically efficient process of mitochondrial oxidative phosphorylation [10]. This phenomenon, which significantly influences the initiation and progression of tumors and subsequent therapeutic strategies, is referred to as the Warburg effect [11]. The basis for this increased glucose uptake is the substantial upregulation of both the expression and activity of glucose transporters (GLUTs) in tumor cells. Once imported, glucose is phosphorylated by HK to form glucose-6-phosphate, which is subsequently isomerized to fructose-6-phosphate by the rate-limiting enzyme GPI. The glycolytic pathway then advances via numerous enzymatic reactions involving GAPDH, PGAM1, PKM2 among others, ultimately leading to pyruvate production [12]. Importantly, lactate dehydrogenase A (LDHA) rapidly reduces pyruvate to lactate, simultaneously regenerating NAD^+ to maintain the elevated glycolytic flux [13].

The aberrant activation of glycolysis not only facilitates tumor progression but also reveals distinct diagnostic and therapeutic opportunities [14]. The increased expression of crucial glycolytic enzymes such as GLUT1, HK2, PKM2, and LDHA, is often associated with a poor clinical prognosis [15]. The inhibition of glycolysis reduces ATP levels, thereby enhancing the efficacy of chemotherapy or radiotherapy and increasing the sensitivity of tumor cells to targeted therapies [16]. Furthermore, the suppression of lactate production or its export can mitigate acidosis in the tumor microenvironment (TME) and alleviate related immunosuppressive conditions, potentially enhancing the effectiveness of immunotherapies such as immune checkpoint inhibitors. Consequently, combinatorial strategies that target glycolysis in conjunction with immunotherapy are becoming research hotspots [17]. The multiomics approach used in our study identified the potent inhibitory effects of XDQ on tumor glycolysis. These findings establish a foundation for expanding the clinical applications of XDQ and open promising and novel therapeutic avenues for treating liver cancer.

Glycolysis is a fundamental pathway for cells for energy acquisition, in addition to it being a pivotal regulator of immune cell function. The energy metabolism profile of immune cells, particularly their dependence on glycolysis, undergoes dynamic

reprogramming across various functional states. This metabolic plasticity significantly influences proliferation, differentiation, cytokine production, and effector functions [18]. Glycolytic intermediates serve as crucial precursors for the synthesis of nucleotides, amino acids, and lipids, thereby facilitating the rapid proliferation, differentiation, and macromolecular biosynthesis required by activated immune cells. In contrast, the Warburg effect seen in tumor cells leads to extensive glucose consumption and lactate production, resulting in an immunosuppressive TME characterized by glucose deprivation, lactate accumulation, and acidosis. Lactate itself can directly inhibit the function of effector T cells and natural killer cells, while simultaneously enhancing the immunosuppressant activity of regulatory T cells and myeloid-derived suppressor cells, as well as impairing the maturation and function of dendritic cells [19]. Consequently, the development of therapeutic agents targeting key glycolytic enzymes (e.g., HK2, PKM2), transporters (e.g., GLUT1), or lactate signaling pathways represents a highly promising immunomodulatory strategy. The inhibition of tumor glycolysis via these approaches has the potential to remodel the immunosuppressive TME, thereby restoring antitumor immunity [20].

In this study, 5 compounds in XDQ were identified, specnuezhenide, prosapogenin A, oleuropein, oxyberberine, and pseudoanisatin, which were found to be bioavailable and capable of entering systemic circulation and target organs. These compounds represent the potential bioactive constituents responsible for the efficacy of XDQ in alleviating liver cancer. The study conducted by Hang Yu et al. demonstrates that specnuezhenide is capable of directly penetrating tumor tissues and inhibiting tumor progression, findings that align with our own research outcomes [21]. Nonetheless, there is currently a lack of direct empirical evidence regarding the regulatory impact of specnuezhenide on tumor glycolysis. In contrast, prosapogenin A has been shown to exert inhibitory effects on malignant tumors, including non-small cell lung cancer and thyroid cancer. Substantial evidence supports its role in modulating ATP metabolism, thereby facilitating pyroptosis in thyroid cancer [22-23]. Oleuropein is recognized for its beneficial effects in diabetes, malaria, and inflammation, and has been previously shown to directly target and inhibit glycolysis,

thereby suppressing the progression of liver cancer [24]. In conclusion, XDQ, a traditional Chinese medicine with a long history of clinical use, possesses well-documented therapeutic efficacy. The identification of 5 bioavailable and organotropic constituents, each with diverse bioactivities including significant anti-tumor effects, further supports the anti–liver cancer effects of XDQ. Importantly, our research findings suggest that the anti-cancer effects of XDQ are mediated through the regulation of tumor glycolysis. Specifically, specnuezhenide, prosapogenin A, and oleuropein, as constituents of XDQ that directly enter the bloodstream and tumor tissues, constitute the material basis for its glycolysis inhibition.

5. Conclusions

The chemical and molecular mechanisms underlying the anti–liver cancer effects of XDQ were successfully elucidated. A total of 66 compounds in XDQ were identified, with 5 compounds showing good bioavailability by entering the bloodstream and accumulating in liver tumors, potentially mediating its therapeutic efficacy. XDQ exhibited a significant anti-tumor effect, with up to 79.64% inhibition of tumor growth at high dosages and without significant toxicity. Comprehensive transcriptomic, proteomic, and in combination with network pharmacology confirmed the primary anti-cancer effect of XDQ, which was by inhibiting the glycolysis, a critical metabolic vulnerability in tumors. Our study further identified specnouezide as the main component of XDQ that targets GPI to inhibit glycolysis. These findings provide a foundation for the development of XDQ-based therapeutic strategies for liver cancer treatment. Future research should aim to validate the synergistic effects of the five compounds identified in this study and explore their molecular targets within the glycolysis.

Declarations

Author contribution

HZC, YJX, and SWJ were responsible for the experimental operation and played

a key role in the manuscript writing and data verification. JCH, HBD and LHC helped to complete part of the experiment. WJJ and DXY are responsible for designing and guiding the experiment. All data were generated in-house, and no paper mill was used. All authors agree to be accountable for all aspects of work ensuring integrity and accuracy.

Conflict of interest

The authors declare that that they have no competing interests.

Ethical Approval and Consent to participate

Animal welfare and experimental procedures strictly follow the guidelines of the Animal Research Committee of Hubei Minzu University (202271), and comply with the ARRIVE (Animal Research: Reporting of In Vivo Experiments) guidelines.

Data Availability

The transcriptomic and proteomic datasets generated and analyzed during the current study are available in the Science Data Bank repository, https://www.scidb.cn/en/anonymous/bkVaN3ph. All other relevant data are included in the article and its Supplementary Information files.

Funding

This research was supported by Hubei provincial Natural Science Foundation of China (2023AFD067); Science Research Program for Young Talents of Hubei Provincial Department of Education (Q20231904); Hubei Province Traditional Chinese Medicine Joint Fund Project (ZY2025L043); Open Fund Project of Hubei Provincial Key Laboratory of Occurrence and Intervention of Rheumatic diseases (PT02314); Initial funding for the Ph.D. of Hubei Minzu University; Provincial Key Laboratory Research Project (2021-06).

Acknowledgements

Not applicable

Reference

[1] Vogel A, Meyer T, Sapisochin G, Salem R, Saborowski A. Hepatocellular carcinoma. Lancet. 2022 Oct 15;400(10360):1345-1362. doi: 10.1016/S0140-6736(22)01200-4.

[2] Bray F, Laversanne M, Sung H, Ferlay J, Siegel RL, Soerjomataram I, Jemal A. Global cancer statistics 2022: GLOBOCAN estimates of incidence and mortality worldwide for 36 cancers in 185 countries. CA Cancer J Clin. 2024 May-Jun;74(3):229-263. doi: 10.3322/caac.21834.

[3] Chick RC, Ruff SM, Pawlik TM. Neoadjuvant systemic therapy for hepatocellular carcinoma. Front Immunol. 2024 Mar 1;15:1355812. doi: 10.3389/fimmu.2024.1355812.

[4] Diao X, Guo C, Jin Y, Li B, Gao X, Du X, Chen Z, Jo M, Zeng Y, Ding C, Liu W, Guo J, Li S, Qiu H. Cancer situation in China: an analysis based on the global epidemiological data released in 2024. Cancer Commun (Lond). 2025 Feb;45(2):178-197. doi: 10.1002/cac2.12627.

[5] Han B, Zheng R, Zeng H, Wang S, Sun K, Chen R, Li L, Wei W, He J. Cancer incidence and mortality in China, 2022. J Natl Cancer Cent. 2024 Feb 2;4(1):47-53. doi: 10.1016/j.jncc.2024.01.006.

[6] Wang M, Jiang S, Yuan H, Zafar S, Hussain N, Jian Y, Li B, Gong L, Peng C, Liu C, Wang W. A review of the phytochemistry and pharmacology of Kadsura heteroclita, an important plant in Tujia ethnomedicine. J Ethnopharmacol. 2021 Mar 25;268:113567. doi: 10.1016/j.jep.2020.113567.

[7] Zhang Y, Hanula JL, Horn S, Jones C, Kristine Braman S, Sun J. Fundamental Host Range of Leptoypha hospita (Hemiptera: Tingidae), a Potential Biological Control Agent of Chinese Privet. Environ Entomol. 2016 Aug;45(4):897-908. doi: 10.1093/ee/nvw062.

[8] Wu S, Tong L, Liu B, Ai Z, Hong Z, You P, Wu H, Yang Y. Bioactive ingredients obtained from Cortex Fraxini impair interactions between FAS and GPI. Free Radic Biol Med. 2020 May 20;152:504-515. doi: 10.1016/j.freeradbiomed.2019.11.022.

[9] Debbage P. Targeted drugs and nanomedicine: present and future. Curr Pharm Des. 2009;15(2):153-72. doi: 10.2174/138161209787002870.

[10] Paul S, Ghosh S, Kumar S. Tumor glycolysis, an essential sweet tooth of tumor cells. Semin Cancer Biol. 2022 Nov;86(Pt 3):1216-1230. doi: 10.1016/j.semcancer.2022.09.007.

[11] Zhong X, He X, Wang Y, Hu Z, Huang H, Zhao S, Wei P, Li D. Warburg effect in colorectal cancer: the emerging roles in tumor microenvironment and therapeutic implications. J Hematol Oncol. 2022 Nov 1;15(1):160. doi: 10.1186/s13045-022-01358-5.

[12] Qiao Q, Hu S, Wang X. The regulatory roles and clinical significance of glycolysis in tumor. Cancer Commun (Lond). 2024 Jul;44(7):761-786. doi: 10.1002/cac2.12549.

[13] Le A, Cooper CR, Gouw AM, Dinavahi R, Maitra A, Deck LM, Royer RE, Vander Jagt DL, Semenza GL, Dang CV. Inhibition of lactate dehydrogenase A induces oxidative stress and inhibits tumor progression. Proc Natl Acad Sci U S A. 2010 Feb 2;107(5):2037-42. doi: 10.1073/pnas.0914433107.

[14] Li Y, Wang W, Xu D, Liang H, Yu H, Zhou Y, Liang J, Sun H, Liu X, Xue M, Ling B, Feng D. PIWIL2/PDK1 Axis Promotes the Progression of Cervical Epithelial Lesions via Metabolic Reprogramming to Maintain Tumor-Initiating Cell Stemness. Adv Sci (Weinh). 2024 Dec;11(48):e2410756. doi: 10.1002/advs.202410756.

[15] Xia P, Zhang H, Lu H, Xu K, Jiang X, Jiang Y, Gongye X, Chen Z, Liu J, Chen X, Ma W, Zhang Z, Yuan Y. METTL5 stabilizes c-Myc by facilitating USP5 translation to reprogram glucose metabolism and promote hepatocellular carcinoma progression. Cancer Commun (Lond). 2023 Mar;43(3):338-364. doi: 10.1002/cac2.12403.

[16] Zhang Y, Ma H, Li L, Sun C, Yu C, Wang L, Xu D, Song X, Yu R. Dual-Targeted Novel Temozolomide Nanocapsules Encapsulating siPKM2 Inhibit Aerobic Glycolysis to Sensitize Glioblastoma to Chemotherapy. Adv Mater. 2024 Jul;36(29):e2400502. doi: 10.1002/adma.202400502.

[17] Rabinowitz JD, Enerbäck S. Lactate: the ugly duckling of energy metabolism. Nat Metab. 2020 Jul;2(7):566-571. doi: 10.1038/s42255-020-0243-4.

[18] Chelakkot C, Chelakkot VS, Shin Y, Song K. Modulating Glycolysis to Improve Cancer Therapy. Int J Mol Sci. 2023 Jan 30;24(3):2606. doi: 10.3390/ijms24032606.

[19] Llibre A, Kucuk S, Gope A, Certo M, Mauro C. Lactate: A key regulator of the immune response. Immunity. 2025 Mar 11;58(3):535-554. doi: 10.1016/j.immuni.2025.02.008.

[20] Du D, Liu C, Qin M, Zhang X, Xi T, Yuan S, Hao H, Xiong J. Metabolic dysregulation and emerging therapeutical targets for hepatocellular carcinoma. Acta Pharm Sin B. 2022 Feb;12(2):558-580. doi: 10.1016/j.apsb.2021.09.019.

[21] Yu H, Xu H, Yang X, Zhang Z, Hu J, Lu J, Fu J, Bu M, Zhang H, Zhai Z, Wang J, Jiang J, Wang Y. Gut microbiota-based pharmacokinetic-pharmacodynamic study and molecular mechanism of specnuezhenide in the treatment of colorectal cancer targeting carboxylesterase. J Pharm Anal. 2023 Sep;13(9):1024-1040. doi: 10.1016/j.jpha.2023.06.012.

[22] Liu Y, Guo Y, Zeng Q, Hu Y, He R, Ma W, Qian C, Hua T, Song F, Cai Y, Zhu L, Ren X, Xu J, Zheng C, Ding L, Ge J, Wang W, Xu H, Ge M, Zheng G. Prosapogenin A induces GSDME-dependent pyroptosis of anaplastic thyroid cancer through vacuolar ATPase activation-mediated lysosomal over-acidification. Cell Death Dis. 2024 Aug 13;15(8):586. doi: 10.1038/s41419-024-06985-z.

[23] Pan Y, Wei J, Qin D, Zhou X, Gao F, Yu L, Feng C, Mi J, Wu J, Law BYK, Wong VKW, Pan H, Liao B, Ren X, Ren F, Wu A. Prosapogenin CP4 exacerbates mitophagy to induce apoptosis via AMPK-mTOR and PINK1/Parkin pathways in A549 cells. Phytomedicine. 2025 Nov 25;148:157333. doi: 10.1016/j.phymed.2025.157333.

[24] Hong Z, Lu Y, Liu B, Ran C, Lei X, Wang M, Wu S, Yang Y, Wu H. Glycolysis, a new mechanism of oleuropein against liver tumor. Phytomedicine. 2023 Jun;114:154770. doi: 10.1016/j.phymed.2023.154770.

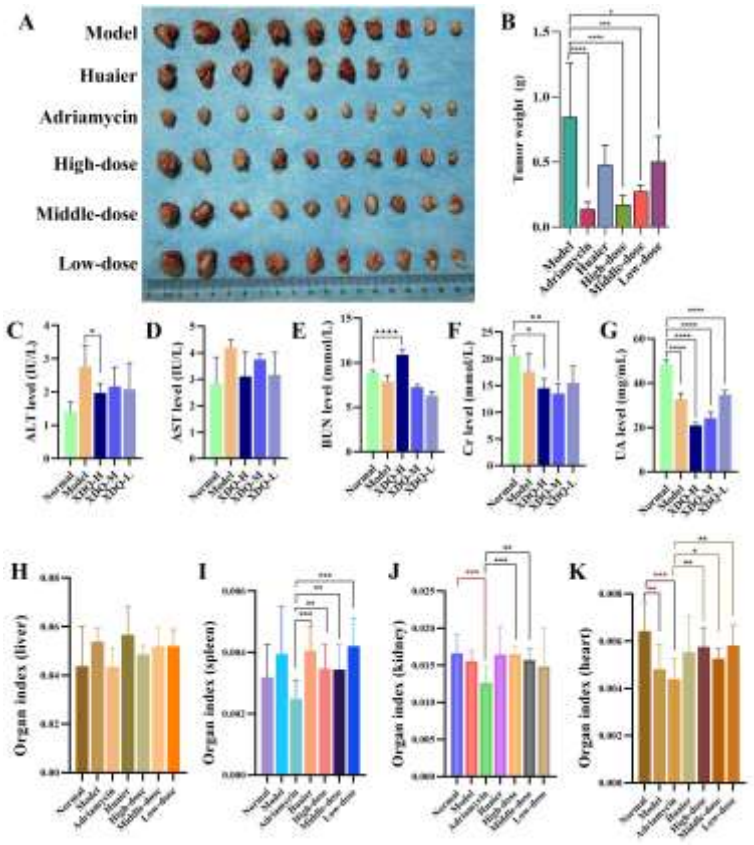

Figure 1 In *vivo* anti-liver cancer activity of XDQ. A: Solid tumor of mice in each experimental group; B: Statistics of tumor weight in each experimental group; Changes in serum alaninetransaminase (C), aspartate transaminase (D), urea nitrogen (E), creatinine (F) and uric acid (G) in serum of mice in each group; Organ indices of liver (H), spleen (I), kidney (J), and heart (K) in each group of mice. *: $p<0.05$, **: $p<0.01$, ***: $p<0.001$, ****: $p<0.0001$.

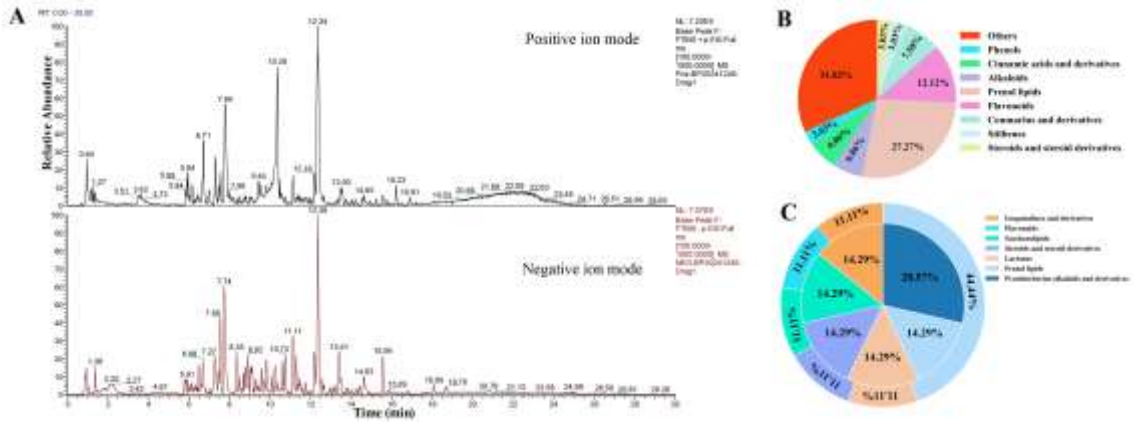

Figure 2 Components analysis of XDQ. A: Total ion chromatogram of XDQ

decoction in UPLC-Q/TOF-MS positive and negative ion modes; B: Pie chart of the classification of the components of XDQ; C: Pie chart showing XDQ components in blood and tumor tissues, the outer circle shows the statistical results of the components entering the blood, and the inner circle shows the statistical results of the components entering the tumor tissue.

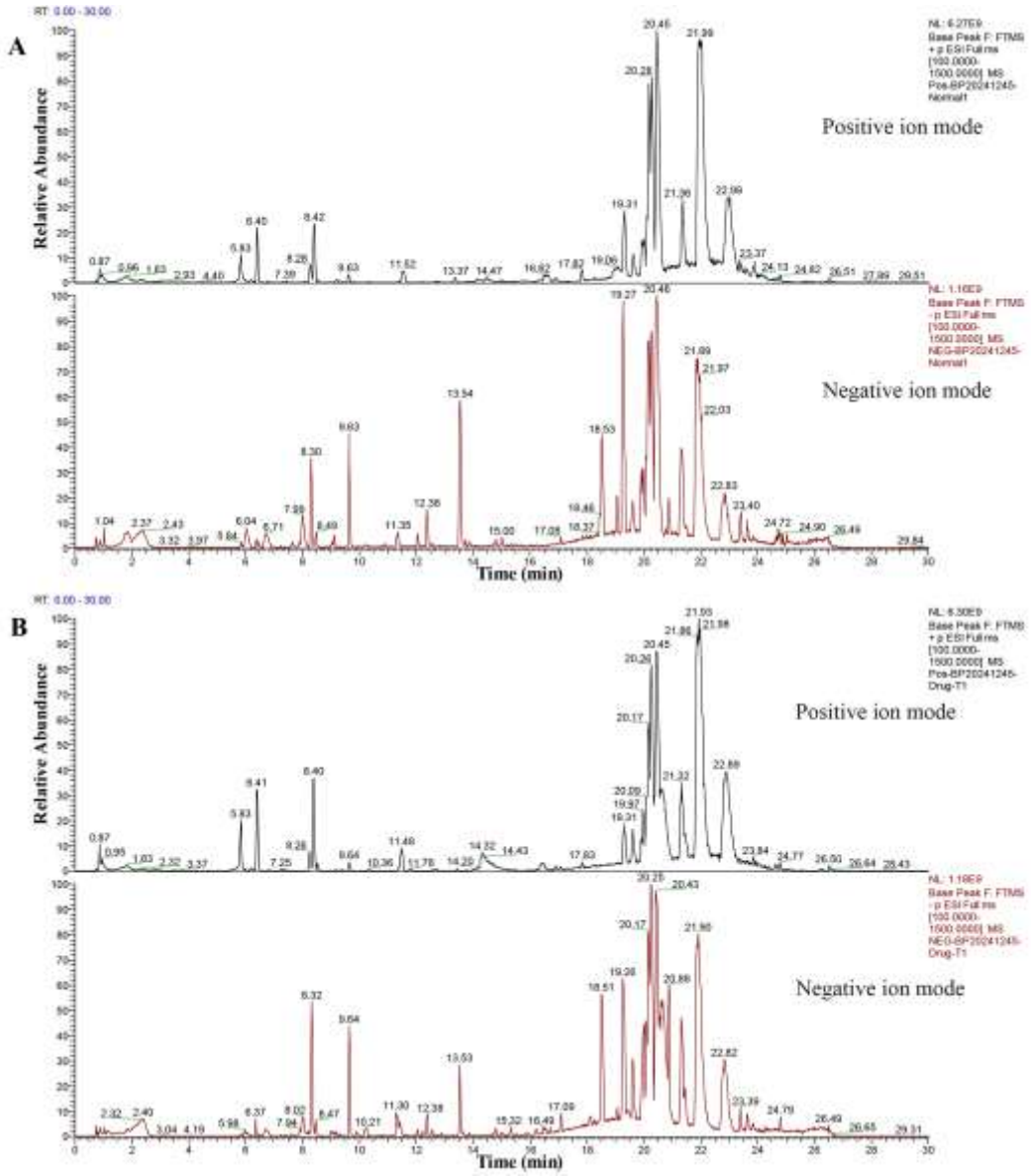

Figure 3 Analysis of XDQ components in the bloodstream. A: UPLC-Q/TOF-MS spectra of blank serum in positive and negative ion modes; B: UPLC-Q/TOF-MS spectra of administered serum in positive and negative ion modes.

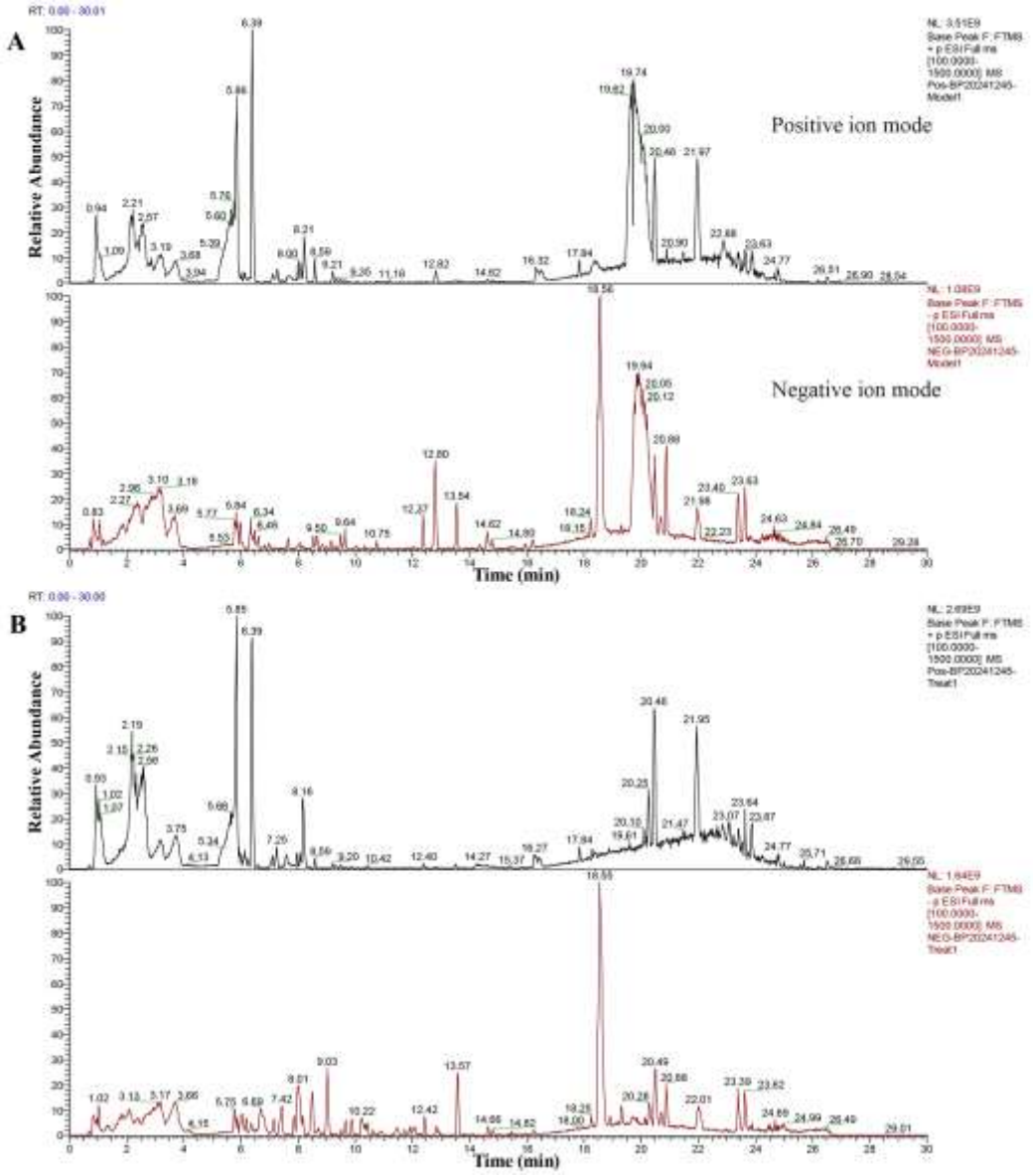

671

672 **Figure 4 Analysis of XDQ components in tumor tissues.** A: UPLC-Q/TOF-MS
673 spectra of tumor tissue extracts from the model group in positive and negative ion
674 modes; B: UPLC-Q/TOF-MS spectra of tumor tissue extracts from high-dose
675 treatment group in positive and negative ion modes.

676

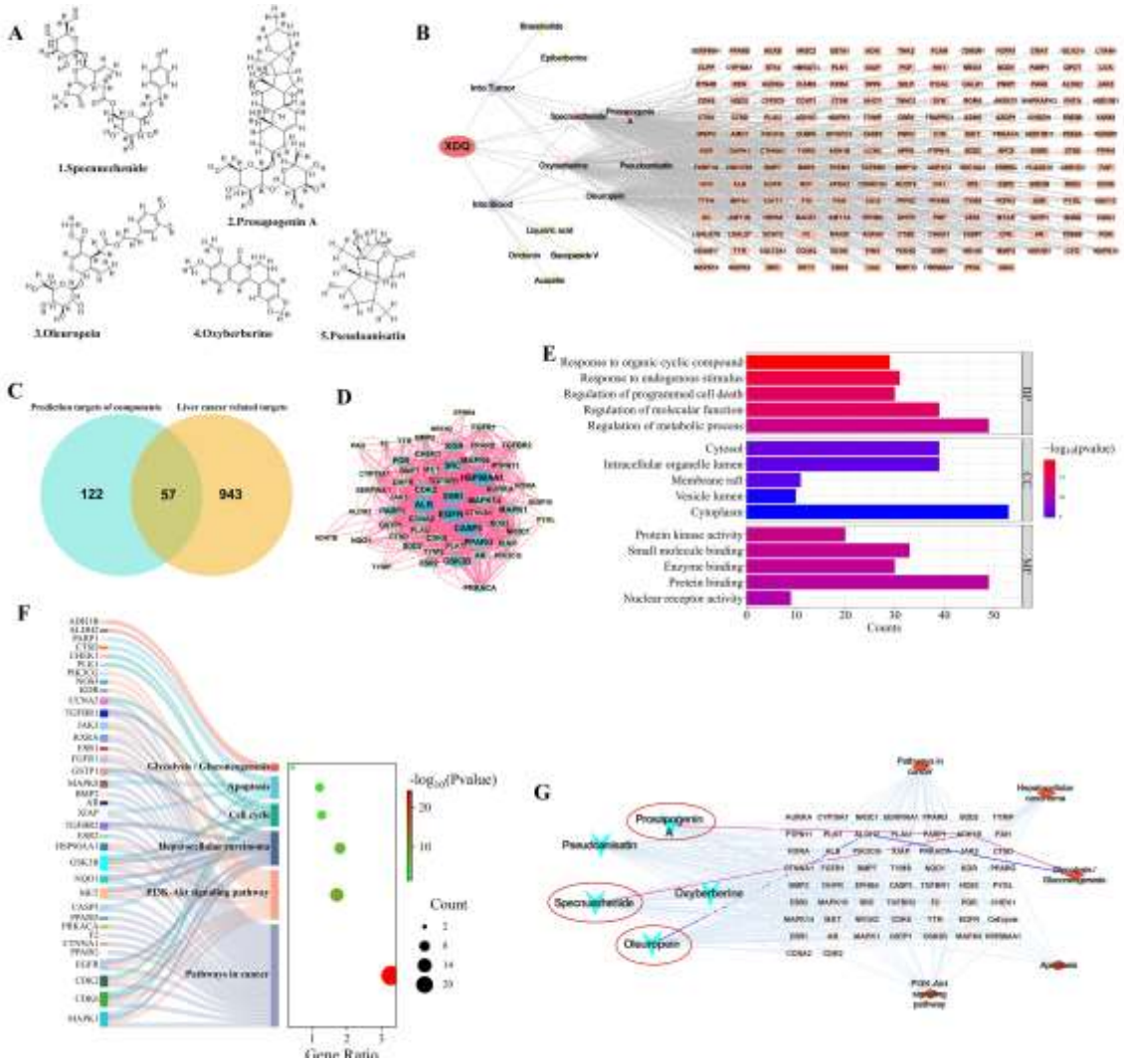

Figure 5 Network pharmacology analysis. A: The chemical structures of five compounds that directly enter blood and tumor tissues; B: Drug-components-targets network; C: The predicted targets of five chemical components that enter both the bloodstream and target organs share 57 common targets with the top 1000 liver cancer related targets; D: PPI interaction results of 57 common targets; E: GO enrichment results of 57 common targets; F: KEGG enrichment results of 57 common targets, G: Components-57 common targets-signaling pathway network, specnuezhenide, prosapogenin A and oleuropein are directly related to glycolysis. KEGG pathway maps were generated using Kanehisa Laboratories' KEGG database.

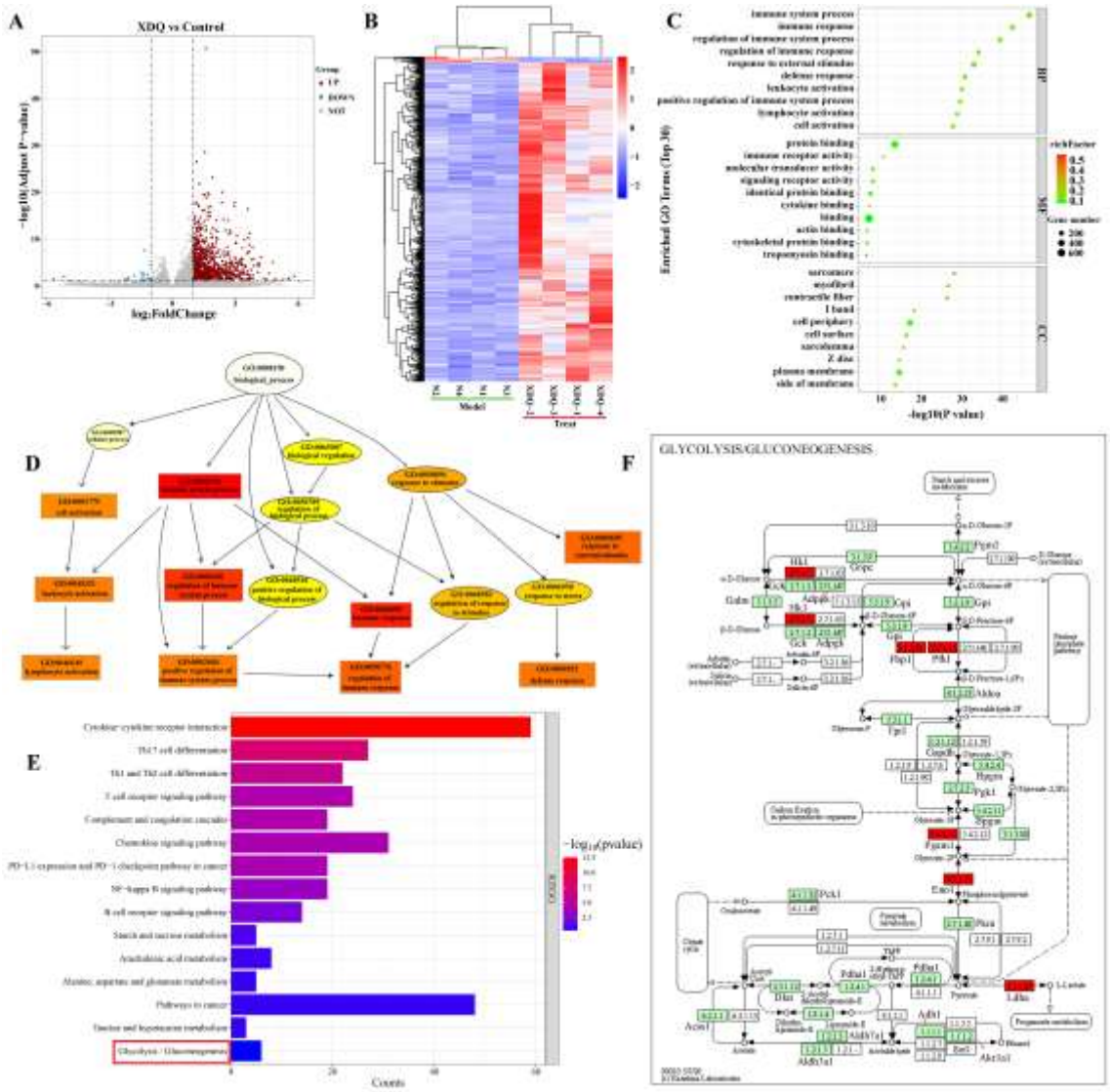

Figure 6 Transcriptomic research on tumor tissues. A: Volcano plot of transcriptome data; B: Gene expression heatmap; C: BP, CC and MF entries of GO enrichment results of differentially expressed genes caused by XDQ; D: Directed acyclic graph of GO enrichment analysis; E: KEGG enrichment results of differentially expressed genes caused by XDQ; F: The KEGG enrichment results showed the glycolysis pathway, with red indicating upregulation of gene expression and green indicating downregulation of gene expression. KEGG pathway maps were generated using Kanehisa Laboratories' KEGG database.

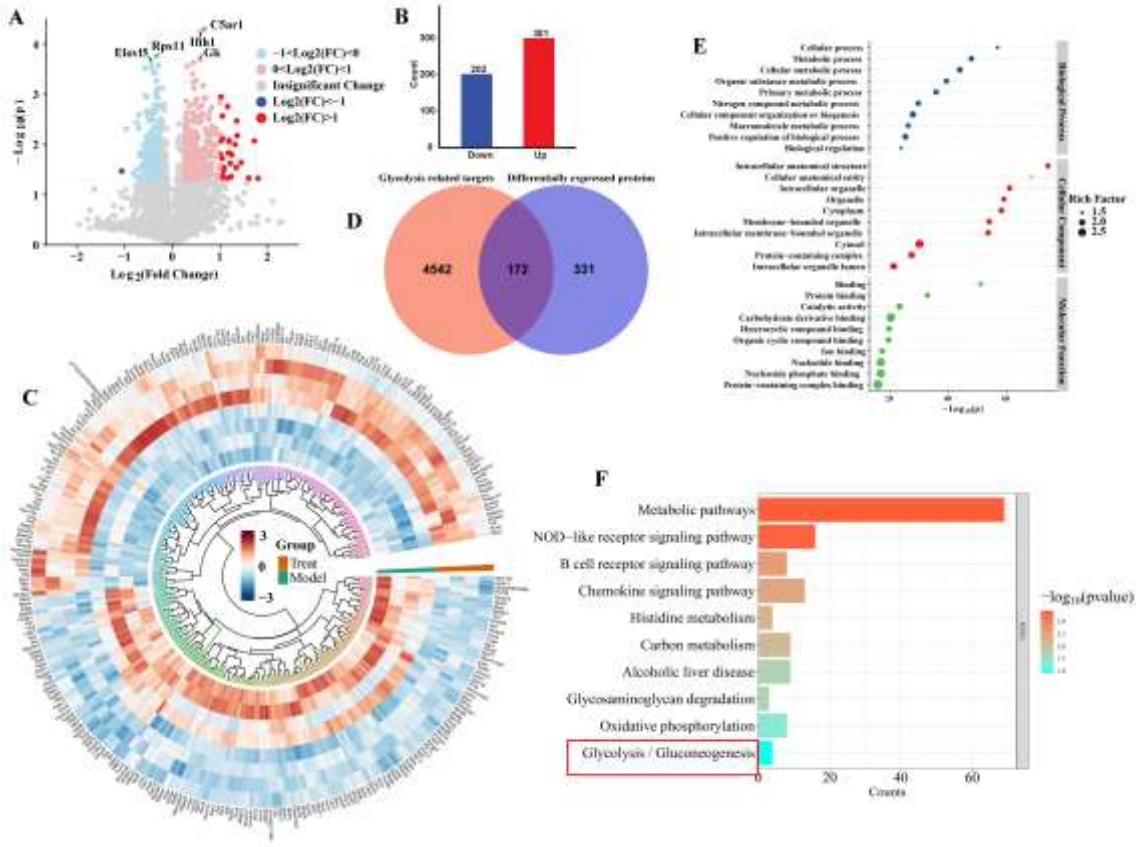

Figure 7 Proteomic research on tumor tissues. A: Volcano plot of proteomic data; B: Statistics of differentially expressed proteins; C: Among the 503 differentially expressed proteins, 172 are related to glycolysis; D: Heatmap of protein expression; E: BP, CC and MF entries of GO enrichment results of differentially expressed proteins caused by XDQ; F: KEGG enrichment results of differentially expressed proteins caused by XDQ. KEGG pathway maps were generated using Kanehisa Laboratories' KEGG database.

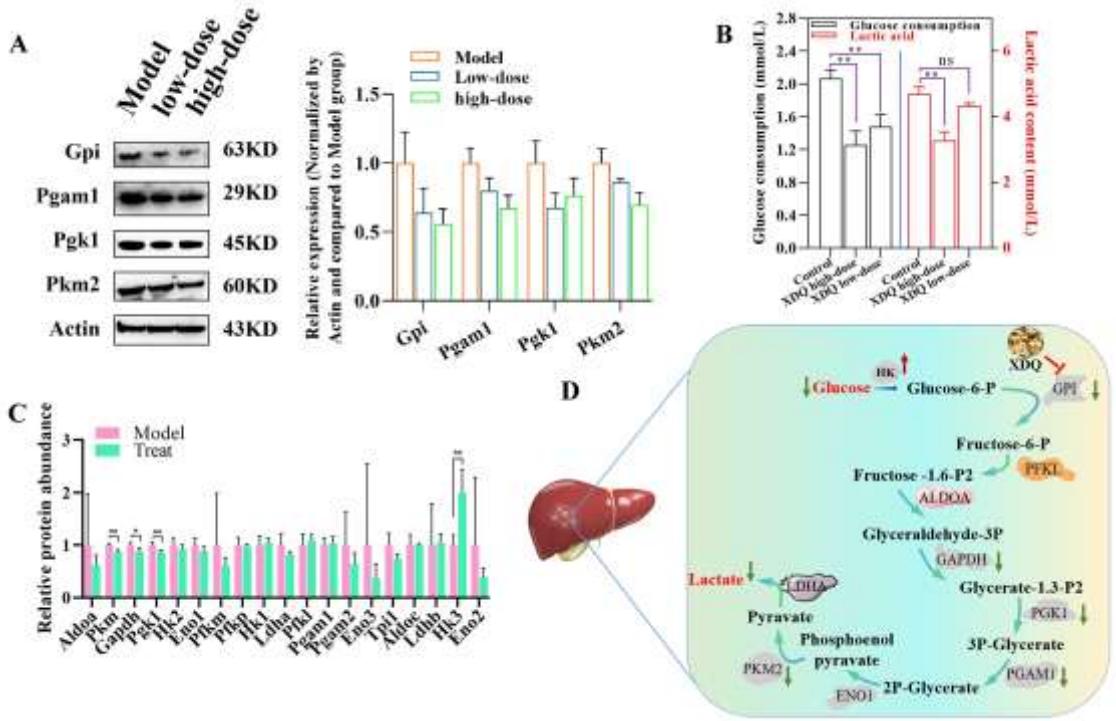

Figure 8 Detection of glycolysis indicators. A: XDQ inhibits the expression of key proteins involved in glycolysis; B: XDQ inhibits the uptake of glucose by tumor tissues and reduces the production of lactic acid; C: The expression of 19 key glycolysis related enzymes in proteomic analysis; D: Potential mechanism of XDQ inhibiting glycolysis in liver cancer. *: $p<0.05$, **: $p<0.01$, ***: $p<0.001$, ****: $p<0.0001$.

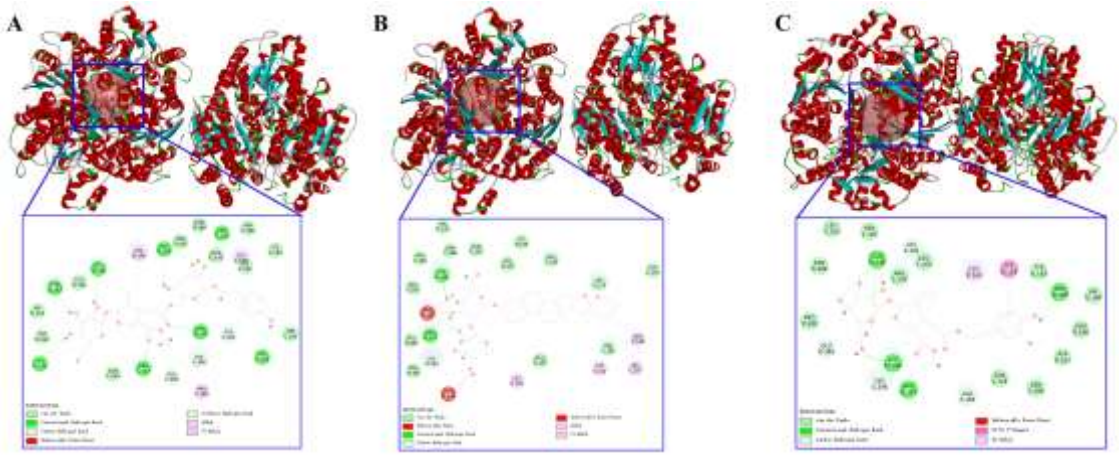

Figure 9 Virtual molecular docking. A: Molecular docking results of Specnuezhenide and GPI; B: Molecular docking results of Prosapogenin A and GPI; C: Molecular docking results of Oleuropein and GPI.

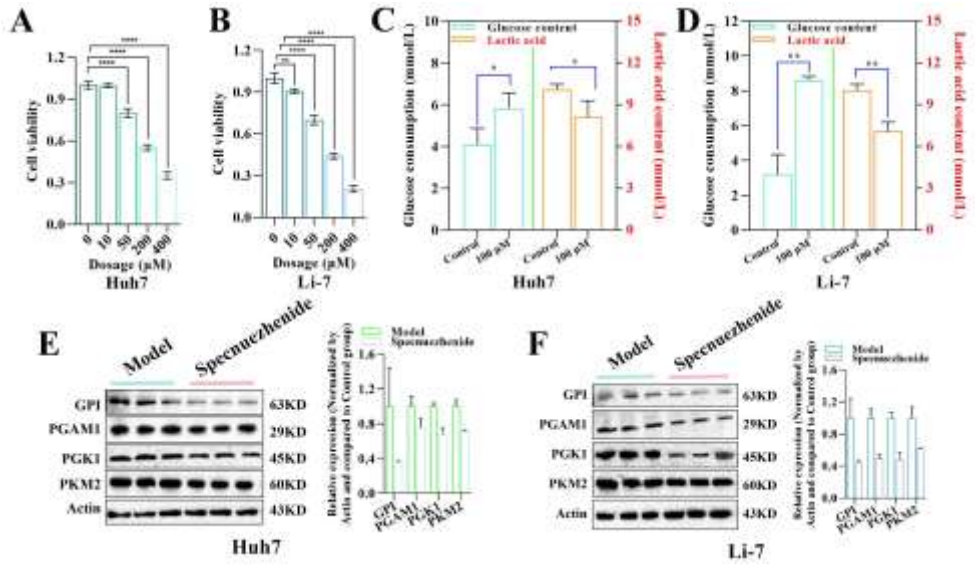

Figure 10 The key active ingredient of XDQ, Specnuezhenide, inhibits glycolysis in liver cancer. A: Specnuezhenide significantly inhibited the proliferation of Huh7 cells; B: Specnuezhenide significantly inhibited the proliferation of Li-7 cells. Compared with the control group, after Specnuezhenide intervention on Huh7 (C) and Li-7 (D) cells, the glucose content in the culture medium increased significantly and the lactic acid production decreased significantly. Specnuezhenide can inhibit the protein expression of GPI, PGAM1, PGK1 and PKM2 in Huh7 cells (E) and Li-7 cells (F). *: $p<0.05$, **: $p<0.01$, ****: $p<0.0001$.

742 **Table 1 Chemical composition in XDQ**

No.	Rt min	Name	Mz	Mass error (ppm)	Formula	MS MS spectrum
1	0.965	Betaine	118.0858	2.0324	$C_5H_{12}NO_2^+$	58.06563, 59.07354, 60.07696, 118.0853
2	1.323	Rhodiocyanoside A	282.0952	1.2762	$C_{11}H_{17}NO_6$	116.99995, 196.0587, 218.08267, 236.09058, 282.09702
3	1.389	Tubuloside A	851.2569	1.2922	$C_{37}H_{48}O_{21}$	347.09042, 527.1546, 671.19983, 689.20062, 851.25153
4	1.799	Oxyberberine	374.0990	2.4325	$C_{20}H_{17}NO_5$	269.05939, 310.08444, 356.08752, 374.09647
5	2.024	Valine	118.0860	2.2018	$C_5H_{11}NO_2$	59.07354, 91.05458, 95.04871, 117.0696, 118.08626
6	2.096	Cordycepin	274.0904	2.4444	$C_{10}H_{13}N_5O_3$	68.92044, 97.02845, 143.03133, 256.12555, 274.10599
7	5.878	Guaiacol	107.0491	1.2144	$C_7H_8O_2$	79.05428, 80.04955, 93.05739, 105.04489, 107.04894
8	5.88	Cinnamic acid	131.0488	1.6788	$C_9H_8O_2$	53.52216, 86.06033, 95.04874, 103.05404, 131.04846
9	6.144	Lycorine	288.1219	3.9219	$C_{16}H_{17}NO_4$	213.07579, 256.0943, 271.11792, 288.12338

10	6.586	Monocrotaline	348.1417	0	$C_{16}H_{23}NO_6$	93.06935, 152.06929, 348.14221	133.06358, 330.13138,
11	6.748	Tabersonine	337.1924	4.0630	$C_{21}H_{24}N_2O_2$	71.95501, 166.72743, 337.13599	84.08035, 256.36282,
12	7.044	Ginsenoside Rh1	683.4393	2.5021	$C_{36}H_{62}O_9$	68.67744, 145.09586, 683.43579	77.06245, 342.21246,
13	7.09	Geniposide	411.1246	3.7215	$C_{17}H_{24}O_{10}$	67.66584, 263.06689, 411.11914	131.04897, 393.10626,
14	7.696	Phlorhizin	459.1256	1.0672	$C_{21}H_{24}O_{10}$	67.97733, 304.07748, 459.13123	216.12256, 330.09741,
15	7.774	Smyrindioloside	447.1249	2.8627	$C_{20}H_{24}O_{10}$	107.04895, 285.07242, 447.12115	233.04147,
16	7.818	Aesculetin	179.0328	3.1999	$C_9H_6O_4$	51.02398, 117.03362, 179.03175	67.62939, 151.03752,
17	7.959	Morin	301.0363	3.3551	$C_{15}H_{10}O_7$	80.96325, 221.07837, 301.03815	130.0851,
18	7.999	Daphylloside	469.1301	3.2400	$C_{19}H_{26}O_{12}$	67.88272, 327.65384, 469.12613	317.08316, 337.08734,
19	8.346	Sinomenine	330.1693	1.9384	$C_{19}H_{23}NO_4$	86.09676, 257.12375, 330.14911	242.10054, 298.12665,
20	9.02	Acacetin	285.07	4.525	$C_{16}H_{12}O$	69.06991,	229.08432,

			45	1	C_5	270.05023, 285.29608	285.07278,
21	9.248	Linderalactone	245.1162	4.0389	$C_{15}H_{16}O_3$	68.33755, 199.11168, 245.07797	185.05975, 218.11621,
22	9.814	Arbutin	295.0789	0.2033	$C_{12}H_{16}O_7$	95.04956, 249.09056, 295.07938	145.06438, 267.09955,
23	9.814	Bruceine D	433.1461	1.9624	$C_{20}H_{26}O_9$	121.06374, 271.09647, 433.14639	209.0945, 289.10455,
24	10.106	Pterostilbene	279.0999	2.6156	$C_{16}H_{16}O_3$	191.08353, 251.10378, 279.10104	219.07866, 264.077,
25	10.118	Baicalin	447.0906	3.6011	$C_{21}H_{18}O_{11}$	61.16382, 120.07933, 377.2106	70.06535, 271.05823,
26	10.189	Gigantol	297.1108	3.5004	$C_{16}H_{18}O_4$	237.08853, 282.08792, 297.10901	265.08548,
27	10.211	Specnuezhenide	709.2278	5.1746	$C_{31}H_{42}O_{17}$	305.09778, 531.185, 709.22455	473.14114, 547.17712,
28	10.289	Prosapogenin A	745.4157	3.1124	$C_{39}H_{62}O_{12}$	59.12354, 70.06538, 745.41193	67.81125,
29	10.422	Pseudoanisatin	321.1305	0.9653	$C_{15}H_{22}O_6$	96.86367, 299.06128, 321.12686	225.789,
30	10.516	Bacopaside V	789.4390	0.6080	$C_{41}H_{66}O_{13}$	56.91029, 86.09599, 789.44519	67.93482, 629.54205,

31	11.29	Epiberberine	359.1109	2.4505	$C_{20}H_{18}NO_4^+$	73.40345, 196.03748, 341.09232, 359.10172	
32	11.552	Ferulic acid	177.0539	0.5083	$C_{10}H_{10}O_4$	89.03846, 117.03354, 145.02791, 162.03072, 177.05359	
33	11.601	Oleuropein	563.1719	2.9121	$C_{25}H_{32}O_{13}$	203.05176, 369.08981, 401.11496, 563.16669	
34	11.618	Atractyloside A	471.2184	3.5016	$C_{21}H_{36}O_{10}$	68.12374, 137.05849, 275.0726, 335.09534, 471.2146	
35	11.668	Protostemotinine	416.2051	4.1806	$C_{23}H_{29}NO_6$	167.06898, 233.0788, 316.15302, 387.14355, 416.202	
36	11.894	Triptolide	383.1449	4.1238	$C_{20}H_{24}O_6$	68.30785, 353.09482, 368.1225, 383.14417	
37	12.171	Toddalolactone	331.1160	2.2349	$C_{16}H_{20}O_6$	67.55145, 244.63152, 271.09241, 331.11227	
38	12.486	Harpagide	387.1253	2.0407	$C_{15}H_{24}O_{10}$	137.05864, 267.08051, 337.10663, 357.12949, 387.13687	
39	12.497	Scoparone	207.0642	4.6845	$C_{11}H_{10}O_4$	147.04315, 151.07474, 179.06833, 192.04172, 207.06447	
40	12.579	Vincristine	825.4069	0	$C_{46}H_{56}N_4O_{10}$	129.10179, 226.11769, 260.19385, 603.23608, 825.40271	
41	12.84	Piperlongumine	340.1155	0.0882	$C_{17}H_{19}NO_5$	262.08563, 280.09351, 322.10715, 340.11462	
42	13.0	Palmatine	352.15	3.805	$C_{21}H_{22}N$	68.6731, 308.12543,	

	36		27	2	O_4^+	322.1062, 352.15027	337.12997,
43	13.778	Umbelliferone	163.0382	4.6001	$C_9H_6O_3$	79.05428, 133.02701, 163.03882	95.04952, 135.04318,
44	13.855	Licoflavone C	339.1213	3.9514	$C_{20}H_{18}O_5$	279.10114, 321.11032, 339.12335	307.09204, 324.09448,
45	13.87	8-Gingerol	345.2046	2.7520	$C_{19}H_{30}O_4$	81.07009, 177.12762, 345.2037	135.07919, 299.1983,
46	13.988	Isoalantolactone	215.1421	4.3692	$C_{15}H_{20}O_2$	133.0634, 173.09505, 215.14102	159.07913, 187.11093,
47	14.049	Obacunone	477.1875	1.6555	$C_{26}H_{30}O_7$	119.04891, 372.13458, 477.18832	175.07472, 417.17416,
48	14.256	Ganoderic acid I	555.2953	4.3941	$C_{30}H_{44}O_8$	335.09009, 508.15784, 555.27747	423.22955, 538.17096,
49	14.271	Isoferulic acid	177.0537	1.8638	$C_{10}H_{10}O_4$	135.04355, 149.05914, 177.05363	145.02797, 162.03075,
50	14.995	Genistin	455.0961	2.7467	$C_{21}H_{20}O_{10}$	151.0378, 370.08035, 455.09918	341.0506, 398.07791,
51	15.384	Brassinolide	503.3341	0.4172	$C_{28}H_{48}O_6$	68.42281, 439.31671, 503.34604	267.15622, 467.31058,

52	15.555	Epicatechin	313.0687	1.6610	$C_{15}H_{14}O_6$	83.04953, 270.04953, 313.06738	253.0471, 298.0433,
53	15.911	Limonin	493.1815	3.6498	$C_{26}H_{30}O_8$	67.87099, 373.1232, 493.17987	235.05527, 434.22586,
54	16.128	Cynaropicrin	369.1293	4.1449	$C_{19}H_{22}O_6$	226.54706, 351.18097, 369.12994	287.11035,
55	16.153	Oridonin	387.1777	0.2583	$C_{20}H_{28}O_6$	67.0545, 167.06871, 387.12961	81.06995, 181.04803,
56	17.282	Nobiletin	403.1372	3.9193	$C_{21}H_{22}O_8$	264.2686, 373.08951, 403.13385	358.06509, 388.11365,
57	18.164	Ganolucidic acid A	499.3073	2.6236	$C_{30}H_{44}O_6$	78.95673, 303.22949, 499.29773	214.04575, 437.30026,
58	18.433	Auraptene	297.1499	0.9086	$C_{19}H_{22}O_3$	59.0118, 230.02354, 297.14789	183.00958,
59	18.529	Paclitaxel	876.3170	3.6174	$C_{47}H_{51}NO_{14}$	239.14084, 531.19672, 876.31232	308.0896, 591.22198,
60	19.352	Triptophenolide	311.1658	1.7676	$C_{20}H_{24}O_3$	79.95555, 96.86373, 311.16473	93.20744, 183.00986,
61	20.978	Liquoric acid	483.3110	0	$C_{30}H_{44}O_5$	78.95673, 255.22893, 483.31155	152.99313, 405.27631,
62	21.0	Tetrandrine	623.31	4.604	$C_{38}H_{42}N$	71.08595,	341.30118,

	66		45	4	$_2O_6$	443.25412, 623.31146	461.26489,
63	24.595	Denudatine	344.2594	2.9338	$C_{22}H_{33}NO_2$	81.07008, 240.26727, 344.25681	109.10132, 298.25323,
64	24.744	Ganoderic acid F	593.2742	3.6071	$C_{32}H_{42}O_9$	431.18127, 461.2283, 593.27179	446.20789, 533.25726,
65	25.427	Schinifoline	258.1842	4.2605	$C_{17}H_{23}NO$	83.08551, 228.13666, 258.18274	215.12872, 243.16118,
66	26.942	Norhygrine	128.1071	0.7806	$C_7H_{13}NO$	70.06541, 84.08109, 128.10689	82.06554, 110.05959,

743

744

745

746 **Table 2 Distribution of components in animal blood and tumor tissues of XDQ**

No.	Name	Formula	Into Blood	Into Tumor
1	Oxyberberine	$C_{20}H_{17}NO_5$	√	√
2	Acacetin	$C_{16}H_{12}O_5$	√	×
3	Specnuezhenide	$C_{31}H_{42}O_{17}$	√	√
4	Prosapogenin A	$C_{39}H_{62}O_{12}$	√	√
5	Pseudoanisatin	$C_{15}H_{22}O_6$	√	√
6	Bacopaside V	$C_{41}H_{66}O_{13}$	√	/
7	Oleuropein	$C_{25}H_{32}O_{13}$	√	√
8	Oridonin	$C_{20}H_{28}O_6$	√	×
9	Liquoric acid	$C_{30}H_{44}O_5$	√	×

10	**Epiberberine**	**$C_{20}H_{18}NO_4^+$**	×	√
11	**Brassinolide**	**$C_{28}H_{48}O_6$**	×	√

Table 3 Molecular docking results of 5 compounds with the key enzyme GPI in glycolysis

Receptor	**LibDockScore with ligand**				
	Specnuezhenide	**Prosapogenin A**	**Oleuropein**	**Oxyberberine**	**Pseudoanisatin**
GPI	**176.613**	**141.631**	**140.191**	**62.170**	**N/A**

Supplementary Files

This is a list of supplementary files associated with this preprint. Click to download.

- TableS1Reagentmaterials.doc
- TableS2Thetop1000livercancerrelatedtargets.xlsx
- TableS357predictedtargetsfor5compounds..xlsx
- TableS4Recordoftumorvolumeintumorbearingmice.xlsx
- TableS5Recordoftumorweightintumorbearingmice.xlsx
- SupplementarymaterialWBrepeats.pdf